Post density functional theoretical studies of highly polar semiconductive $Pb(Ti_{1-x}Ni_x)O_{3-x}$ solid solutions: Effects of cation arrangement on band gap

G. Y. Gou,[1] J. W. Bennett,[2] H. Takenaka,[1] and A. M. Rappe[1]

[1]*The Makineni Theoretical Laboratories, Department of Chemistry, University of Pennsylvania, Philadelphia, Pennsylvania 19104-6323, USA*

[2]*Department of Physics and Astronomy, Rutgers University, Piscataway, New Jersey 08854-8019, USA*

(Received 11 February 2011; revised manuscript received 1 April 2011; published 18 May 2011)

We use a combination of conventional density functional theory (DFT) and post-DFT methods, which include the local density approximation plus Hubbard U (LDA + U), PBE0, and self-consistent GW, to study the electronic properties of Ni-substituted $PbTiO_3$ (Ni-PTO) solid solutions. We find that LDA calculations yield unreasonable band structures, especially for Ni-PTO solid solutions that contain an uninterrupted NiO_2 layer. Accurate treatment of localized states in transition-metal oxides such as Ni-PTO requires post-DFT methods. B-site Ni/Ti cation ordering is also investigated. The B-site cation arrangement alters the bonding between Ni and O, and therefore strongly affects the band gap (E_g) of Ni-PTO. We predict that Ni-PTO solid solutions should have a direct band gap in the visible light energy range, with polarization similar to the parent $PbTiO_3$. This combination of properties makes Ni-PTO solid solutions promising candidate materials for solar energy conversion devices.

DOI: 10.1103/PhysRevB.83.205115 PACS number(s): 77.84.Lf, 71.15.−m, 71.20.−b

I. INTRODUCTION

The bulk photovoltaic effect (BPVE) has been observed in ferroelectric perovskite oxides such as $Pb(Zr_{1-x}Ti_x)O_3$,[1–3] $LiNbO_3$,[4] and $BaTiO_3$.[5] This effect has attracted an increasing research interest because of its potential application for solar energy conversion devices. As incident light is absorbed by a single-phase ferroelectric material, the photoexcited electrons and holes are spontaneously separated, preventing recombination, and producing a photovoltaic effect. One ferroelectric material extensively studied for this purpose is $BiFeO_3$. It has a strong polarization $\approx$0.9 C/m^2 (Refs. 6 and 7) and a direct band gap $\approx$ 2.67 eV.[8] Recent experiments have demonstrated the BPVE of $BiFeO_3$ under visible incident light.[9–11] However, $BiFeO_3$ is one of very few ferroelectric materials that have both large spontaneous polarization and small E_g. Most solid oxide ferroelectrics are wide-gap insulators ($E_g > 3.0$ eV) that absorb very little of the visible spectrum.

Recent theoretical work on $Pb(M_xTi_{1-x})O_{3-x}$ perovskite solid solutions (M = Ni, Pd, and Pt) provides a promising strategy for designing highly polar semiconducting oxides.[12,13] By substituting the B-site Ti with an O-vacancy-stabilized d^8 M^{2+} cation, the resulting system displays a decreased E_g when compared to $PbTiO_3$ (PTO) while retaining a large polarization. Of these proposed materials, Ni-PTO solid solutions possess great potential for practical solar applications, as they can be synthesized from relatively inexpensive raw materials. However, due to the strongly correlated Ni-3d electrons, Ni-PTO has a complex electronic structure that is not captured by standard local density approximation (LDA) calculations.[14] In this study, we explore the electronic structure of Ni-PTO solid solutions with post density functional theory (post-DFT) calculations, including the local density approximation plus Hubbard U (LDA + U), the Perdew-Burke-Ernzerhof hybrid functional (PBE0), and self-consistent GW. We predict the band gap and other electronic properties for Ni-PTO solid solutions of various compositions and B-site orderings to guide future experimental synthesis and measurement.

II. METHODOLOGY

We perform first-principles calculations with a plane-wave basis set, as implemented in the QUANTUM-ESPRESSO[15] and ABINIT[16] codes. The LDA exchange-correlation functional is used for structural relaxations, with a 6 × 6 × 6 Monkhorst-Pack k-point grid[17] and a 50 Ry plane-wave cutoff. All atoms are represented by norm-conserving[18] optimized nonlocal[19] pseudopotentials, generated with the OPIUM code.[20] The electronic contribution to the polarization is calculated following Berry's phase formalism.[21,22]

Several supercell configurations are used, including 1 × 1 × 2 and 1 × 1 × 3 layered structures [with B-cation alternation along the (001) direction], rocksalt (Pb_2NiTiO_5), and $\sqrt{2} \times \sqrt{2} \times 2$ and 2 × 2 × 2 structures (Ni-O_5 cages are separated by Ti-O_5 cages). By studying these configurations, the effects of different compositions and B-site cation orderings can be investigated. Post-DFT methods are then applied to these Ni-PTO systems. In the next section, we briefly describe each post-DFT method to facilitate comparison of results obtained with each method.

III. RESULTS AND DISCUSSION

A. Post-DFT methods

Before applying post-DFT methods to Ni-PTO, we study its parent materials—tetragonal $PbTiO_3$ and cubic NiO—as reference systems to evaluate the performance of post-DFT methods for related materials. We do so because it is known that the Kohn-Sham (KS) band gap determined by the conventional LDA method is systematically underestimated by 50%–100%.[23,24] To improve the quality of the electronic-structure description of Ni-PTO, especially the treatment of correlation for the localized Ni-3d orbitals, we employ LDA + U, the PBE0 hybrid functional, and self-consistent GW (sc-GW) methods.

1. LDA + U

The LDA + U method is a computationally inexpensive way to improve the DFT-LDA band gap. A simplified version of the rotationally invariant formulation of the LDA + U method[14] is employed in the present work, where U is assigned to be the value of the spurious curvature of the total energy of the system with respect to the variation in the number of electrons (n_i) in a localized orbital.[25] The effective interaction parameter U is determined by the change of orbital occupations n_i with respect to an external potential ζ_j projected onto the corresponding localized level:

$$U = \left(\chi_0^{-1} - \chi^{-1}\right)_{ii}, \quad \chi_{ij} = \frac{dn_i}{d\zeta_j}. \tag{1}$$

Here the χ_{ij} are the elements of the linear-response matrix, n_i is the occupation number of the localized levels at site i, and ζ_j represents the potential shift applied on the localized orbital at site j. The screened response matrix χ includes all screening effects from the crystal environment, which is associated with the localized electrons, and χ_0 (the unscreened response matrix) contains nonscreening effects of the total energy of the noninteracting KS states associated with the system. The latter term can be computed from the first iteration in the self-consistent cycle.

Tetragonal $PbTiO_3$ is selected as an example for detailed study. A $2 \times 2 \times 2$ $PbTiO_3$ supercell is used, because it is large enough to give a converged linear-response calculation of U. Figure 1 displays the calculated U values for Pb and Ti atoms of $PbTiO_3$. In the rotationally invariant LDA + U method, on-site interaction energy $E_U \propto U \cdot [\lambda(1-\lambda)]$ (here λ refers to the normalized orbital occupation number: λ is equal to 1 for a fully occupied orbital and 0 for an empty orbital). For fully occupied orbitals such as Pb $5d$, $\lambda = 1$, so on-site correction has no effect. As displayed in Fig. 1(a), the number of electrons in the Pb $5d$ orbitals will not change with respect to the external potential ζ, so $U = 0$ eV. Ti has partially filled $3d$ orbitals, so it has a nonzero U value.

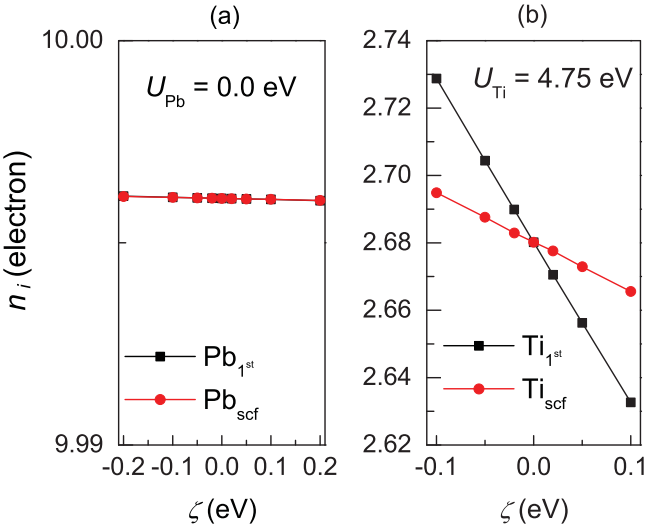

FIG. 1. (Color online) The occupation number (n_i) of localized d orbitals for Pb and Ti in $PbTiO_3$, with respect to potential shift ζ. Shown as (black) squares are the values obtained using self-consistent-field (scf) relaxation, and shown as (red) circles are those without (1st), for constructing χ and χ_0, respectively.

TABLE I. Hubbard U terms (in eV) for Ni and Ti in $PbTiO_3$, NiO, and Ni-PTO solid solutions, obtained with the linear-response approach.

Composition	U_{Ti}	U_{Ni}
$PbTiO_3$	4.75	
NiO		5.70
layered Pb_2NiTiO_5	4.85	9.31
rocksalt Pb_2NiTiO_5	4.85	8.92
$1 \times 1 \times 3$ $Pb_3NiTi_2O_8$	4.75	9.35
$\sqrt{2} \times \sqrt{2} \times 2$ $Pb_4NiTi_3O_{11}$	4.75	8.86
$2 \times 2 \times 2$ $Pb_8NiTi_7O_{23}$	4.77	8.91

Following the above procedure, using the self-consistent linear-response method, as implemented in QUANTUM ESPRESSO, the Hubbard U terms for Ti and Ni in NiO, PTO, and all Ni-PTO solid solutions can be determined (see Table I).

2. PBE0 hybrid density functional with exact exchange

DFT-LDA does not include exact exchange. This is unlike the PBE0 functional, which includes a linear combination of exact-exchange and GGA-PBE exchange (where GGA denotes generalized-gradient approximation).[26] The electron correlation term is the same as that of the PBE functional:[27]

$$E_{xc}^{\mathrm{PBE0}} = \alpha E_x + (1-\alpha)E_x^{\mathrm{PBE}} + E_c^{\mathrm{PBE}}, \tag{2}$$

where α is the fraction of exact exchange. As PBE0 includes a portion of exact exchange, it can greatly reduce the self-interaction error of the local spin density approximation (LSDA) or the GGA functional, and therefore it greatly improves the calculated band gap for most semiconductors and insulators.[27] However, due to the long-range nature of the exact-exchange interaction and resultant large computational cost (about one to two orders of magnitude more than LDA in the present work), PBE0 calculations are mainly applied to periodic systems with small unit cells, such as those described in the present study.[28]

In the original PBE0 functional, $\alpha = 0.25$. However, it is argued that there is no universal α that is applicable for all materials.[29] To predict band-gap values for new materials more accurately, it is considered useful to select an α that yields accurate band gaps for the relevant prototype systems. Figure 2

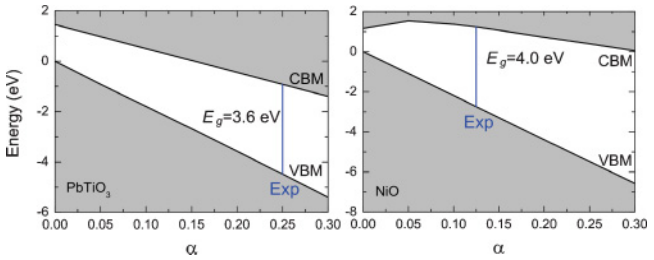

FIG. 2. (Color online) Valence-band maximum (VBM) and conduction-band minimum (CBM) vs PBE0 functional exact-exchange fraction α for $PbTiO_3$ and NiO. Vertical lines represent the experimental band gaps, illustrating how α_0 is chosen (see Table II).

TABLE II. Band gaps (in eV) of $PbTiO_3$ and NiO, calculated using LDA, PBE0 (with the optimal fraction of exact exchange α_0), and sc-GW methods.

	LDA	PBE0 (α_0)	sc-GW	Expt.
$PbTiO_3$	1.46	3.50 (0.25)	3.90	3.60 (Ref. 30)
NiO	1.16	3.98 (0.125)	4.14	4.0–4.3 (Refs. 31 and 32)

shows the α dependence of the conduction- and valence-band edges of $PbTiO_3$ and NiO. Comparing with experimental band-gap values, we obtain an optimal $\alpha_0 = 0.25$ for $PbTiO_3$ and 0.125 for NiO (Fig. 2 and Table II).

3. *Self-consistent GW*

It is widely believed that the self-consistent GW method is the most accurate way to obtain electronic band structures, since it includes both the nonlocality and dynamical correlations absent in DFT-LDA. Therefore, obtaining the self-energy, Σ, is the key quantity of any GW calculation. It was shown by Hedin that the self-energy can be represented as a product of the Green's function G and the screened Coulomb interaction W, $\Sigma = iGW$.[33]

Since our system has a complicated electronic band structure, in which the band gap is dictated by the bonding interactions between the correlated Ni 3d states and O 2p states, the self-consistent GW (sc-GW) method probably gives the most accurate quasiparticle (QP) electronic structures of Ni-PTO.

Following the methodology developed by Lebegue *et al.*,[34] we employ the contour deformation method,[35,36] as implemented in ABINIT, to perform the numerical integral for the self-energy. Within this scheme, the contour of the frequency integral for self-energy is deformed into integrals along the imaginary and real axes. The numerical integral along the imaginary axis can be evaluated by Gaussian quadrature. We find that integrating up to 114 eV and using 10 quadrature points yields converged results for the imaginary axis. The real axis integral is calculated by summing values of the Coulomb screening at a uniform mesh of frequencies, with a mesh spacing of 1.25 eV, from 0 to 120 eV.

This upper limit of real axis integration is chosen from spectral function data[35,36] (electron-energy-loss data in the present work), since the correlation part of the self-energy can be represented by a spectral function.

Due to the expensive computational cost (three to four orders of magnitude more than DFT-LDA in the present work), we restrict sc-GW calculations to only one Ni-PTO system, the rocksalt structure. For this configuration, 400 bands are included, with a plane-wave cutoff of 25 Ha for the QP and LDA states, and a $2 \times 2 \times 2$ Monkhorst-Pack k-point grid.[17] As LDA calculations can qualitatively predict a correct semiconducting ground state for rocksalt Ni-PTO (Fig. 6), we choose to represent the initial QP wave functions in the basis set of LDA wave functions. QP band gaps are converged to within 0.05 eV.

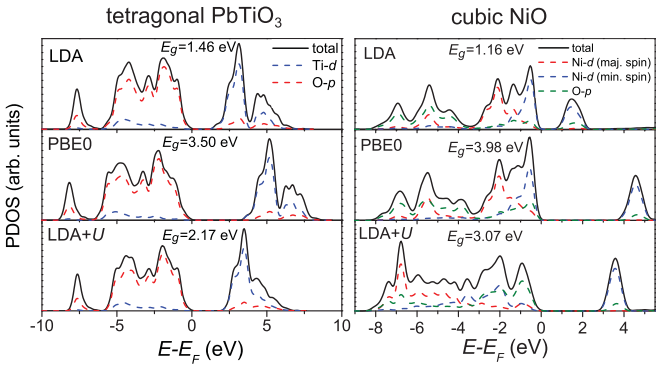

FIG. 3. (Color online) Band-gap values and orbital-resolved PDOS of tetragonal $PbTiO_3$ and cubic NiO using LDA, PBE0, and LDA + U. For PBE0 calculations, the optimal α_0 values are used.

B. Comparison of results for parent end members

Figure 3 shows the projected density of states (PDOS) for tetragonal $PbTiO_3$ and cubic NiO, calculated with the LDA, PBE0, and LDA + U methods, from which we can evaluate the accuracy of each post-DFT method. Experimental studies show that tetragonal $PbTiO_3$ is an insulator with an indirect band gap ($X \rightarrow \Gamma$) of 3.60 eV.[30] LDA severely underestimates this band-gap value by more than 50%. The LDA + U method gives a better band-gap value than the LDA, but it is still lower than PBE0, which comes closest to experiment. This is because the exact exchange in PBE0 is applied to all states, whereas the Hubbard U of LDA + U directly acts *only* on the localized Ti-3d orbitals. Also, when compared to PBE0, LDA + U significantly alters the PDOS for $PbTiO_3$, especially for Ti-3d and O-2p states.

NiO is an antiferromagnetic insulator with an experimentally measured band gap between 4.0 and 4.3 eV.[31,32] As shown in Fig. 3, LDA predicts a band gap of 1.16 eV and LDA + U predicts 3.07 eV, while PBE0 (with $\alpha_0 = 0.125$) reproduces the experimental band gap. For both LDA and PBE0 functionals, the PDOS has a clear split between majority-spin Ni t_{2g} and e_g orbitals, while the band gap of the system falls between occupied minority-spin t_{2g} and empty e_g orbitals. Applying the Hubbard U to the Ni-3d orbitals increases the NiO band gap, relative to the LDA. However, LDA + U predicts Ni-d spectral weight located at a relatively low energy (2–8 eV below E_F). This is in contrast to both experimental photoemission spectra[37] and theoretical dynamical mean-field theory (DMFT) results.[38] These studies suggest that there should be a strong Ni-d contribution to the valence band of the system. Though LDA + U does predict a larger band gap than DFT-LDA, it does not reproduce the salient aspects of the experimental valence-state spectrum of NiO.

C. Electronic properties of Pb_2NiTiO_5 solid solutions

We begin our study of Ni-PTO with the smallest supercell configuration: Pb_2NiTiO_5. In this solid solution, half of the Ti^{4+} cations are replaced by O-vacancy-stabilized Ni^{2+} cations.[12] This polar substitution will generate a $V_O^{\cdot\cdot}$ and Ni''_{Ti} defect pair (in Kröger-Vink notation[39]), where the lowest-energy configuration corresponds to the local dipole parallel to the overall polarization ($\vec{P}$). The Ni-PTO structure is

tetragonal, with a large polarization similar to the parent $PbTiO_3$ (Table IV). After replacing Ti^{4+} with Ni^{2+}, the remaining apical O will move away from Ni^{2+}, making Ni coordination nearly square planar. Since this O atom shifts opposite the cations, it further increases $\vec{P}$. For Pb_2NiTiO_5, two different B-site cation orderings are studied: (i) $1 \times 1 \times 2$ layered and (ii) rocksalt Ni-PTO.

Layered Ni-PTO is structurally similar to the planar nickelate $SrNiO_2$. A previous theoretical study of $SrNiO_2$ predicted it to be a diamagnetic insulator with fully occupied d_{xz}, d_{yz}, d_{xy}, and d_{z^2} orbitals, leaving $d_{x^2-y^2}$ empty.[40] Accordingly, since layered Ni-PTO is a nickelate with planes of Ni^{2+} ions, we anticipate that it should have an insulating ground state.

Figure 4(a) shows the band structure for layered Ni-PTO along high-symmetry directions in the Brillouin zone (BZ). The LDA band structure reveals a two-dimensional character: the energy bands are highly dispersive in the k_x-k_y plane, but show a very weak z-axis dispersion along Γ-Z. One strongly dispersive band [dashed line in Fig. 4(a)] crosses E_F, making the system metallic in LDA. This band is chiefly composed of Ni-$3d_{x^2-y^2}$ and O-$2p$. Isosurfaces for this band at Γ, X, and M points are displayed in Fig. 4(b). There is a pronounced hybridization between Ni-$d_{x^2-y^2}$ and O-p, as the lobes from Ni-$d_{x^2-y^2}$ are directed toward the four O ions. Specifically, the wave functions at X and M consist of O(p_x)-Ni($d_{x^2-y^2}$)-O($s + p_z$) and O(p_x)-Ni($d_{x^2-y^2}$)-O(p_y) orbital combinations, respectively, both of which display antibonding character. However, there is a strong bonding profile between Ni-$d_{x^2-y^2}$ and O-p_z at the Γ point [Ni red (blue) to O red (blue) lobes], which indicates that electron density is shared between O-$2p$ and Ni-$d_{x^2-y^2}$ orbitals, again according to LDA calculations.

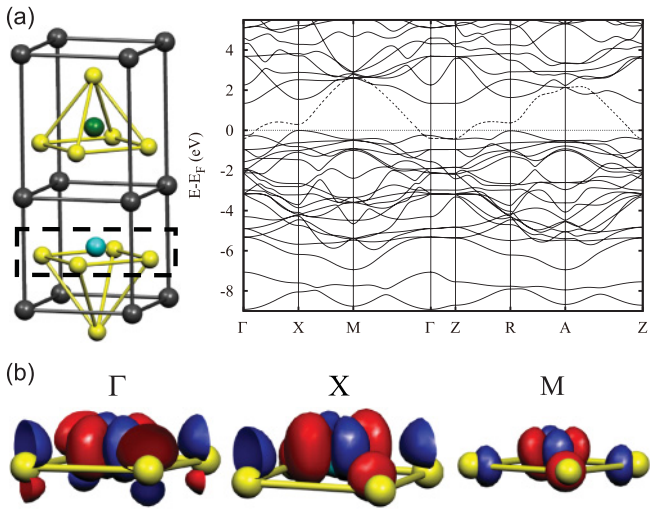

FIG. 4. (Color online) (a) Atomic structure of layered Pb_2NiTiO_5 and its DFT-LDA calculated electronic band structure. The band that crosses the Fermi level is shown as a dashed line. (b) The wave-function isosurfaces are plotted for this band at Γ, X, and M. For clarity, only the isosurface near the Ni-O_2 plane of the band indicated by the dashed lines in (a) is plotted. The isosurface values are $\pm$ 0.04 $e/$Å^3 (red and blue surfaces). The plots illustrate which atomic orbitals compose each eigenstate: Γ: O(p_z)-Ni($d_{x^2-y^2}$)-O(p_z), X: O(p_x)-Ni($d_{x^2-y^2}$)-O($s + p_z$), and M: O(p_x)-Ni($d_{x^2-y^2}$)-O(p_y). This series of images shows the drastic change in bonding from Γ to X to M. Pb, Ti, Ni, and O atoms are represented as gray, green, cyan, and yellow spheres, respectively.

LDA calculations show that for layered Ni-PTO, the band gap is zero. We find that in LDA calculations, the energy level of the Ni-$d_{x^2-y^2}$ orbital is quite low, permitting this low-lying orbital to bond with O-p_z orbitals. This enhancement of the bonding interaction between Ni-$3d_{x^2-y^2}$ and O-$2p$ causes LDA to predict a metallic ground state for layered Ni-PTO.

In our LDA + U calculations, applying the Hubbard U term to the Ni-$3d$ orbitals, in a self-consistent linear-response calculation,[25] yields a split between occupied and unoccupied Ni-$3d$ states. This provides a better description of E_g for Ni-PTO, relative to LDA. However, the PBE0 hybrid density functional, which includes exact-exchange energy, can significantly improve the description of E_g of ferroelectric oxides.[41] To obtain the most realistic results from a PBE0 calculation, the optimal exact-exchange mixing fraction α from relevant prototype systems should be used. Unlike $PbTiO_3$, with E_g between occupied O-$2p$ and empty Ti-$3d$ states, both Ni-PTO and NiO have E_g between occupied and unoccupied Ni-d states. Therefore, we use NiO as our prototype parent system of Ni-PTO, and select $\alpha = 0.125$ for PBE0 calculations of Ni-PTO. A comparison of the eigenvalues at Γ obtained for the Ni $3d$-states using LDA, LDA + U, and PBE0 is presented in the supplementary material.

Though the most computationally demanding of our post-DFT methods, the many-body GW approach is considered the most reliable first-principles method to obtain electronic band structure, and it has been successfully applied to many kinds of perovskite oxides.[42–46] In our present work, we also employ this method for the ground-state calculation of rocksalt Ni-PTO, obtaining a band gap of 1.83 eV. PBE0 predicts a value of 1.71 eV, improving upon the results obtained by LDA (0.69 eV) and LDA + U (1.59 eV), much closer to the sc-GW result.

Figure 5(a) shows the PDOS of Ni-$3d$ in layered Ni-PTO from LDA, LDA + U, and PBE0 calculations. In both the LDA + U and PBE0 PDOS, the Ni-$d_{x^2-y^2}$ band lies above E_F, leading to weaker bonding between Ni-$d_{x^2-y^2}$ and O-$2p$ [Fig. 5(b)]. Unlike LDA, which yields a metallic ground state for layered Ni-PTO, LDA + U and PBE0 predict an intrinsic semiconductor. Since the LDA + U and PBE0 results agree and are more consistent with the Ni-d orbital paradigm in diamagnetic insulating $SrNiO_2$,[40] we consider LDA + U and PBE0 to be more accurate than LDA, and we predict that layered Ni-PTO is a semiconductor.

The calculated PDOS shown in Fig. 5 also shows other prominent features. As a result of the hybridization between Ni and its planar coordinated O, the occupied Ni-d orbitals, such as d_{xz}, d_{yz}, and d_{z^2}, have a large bandwidth of 2 eV (both LDA and PBE0 results). As the Ni ion is shifted up, away from the oxygen plane, the hybridization between Ni-d_{z^2} and O-p_z can give rise to bonding and antibonding states. The double peaks in the d_{xz} and d_{yz} states should correspond to bonding and antibonding states, which come from the hybridization between Ni-d_{xz} (d_{yz}) and O-p_x (p_y) (for details, see the supplementary material). The strong hybridization between Ni and planar O ions indicates the covalency of Ni-O bonds in layered Ni-PTO.

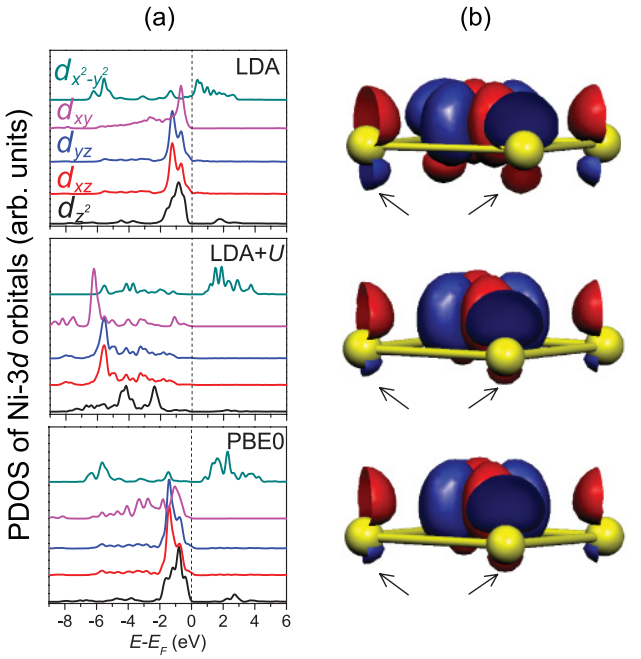

FIG. 5. (Color online) PDOS for Ni-3d and corresponding wave-function isosurface for Ni-$d_{x^2-y^2}$ orbital (at Γ) in layered Pb_2NiTiO_5, calculated using LDA, LDA + U, and PBE0 hybrid density functionals, respectively. Compared to LDA, LDA + U and PBE0 predict smaller downward red (blue) lobes around planar O atoms (see arrows), indicating there is more O s-p hybridization and a weaker bonding interaction between Ni-$d_{x^2-y^2}$ and O-2p.

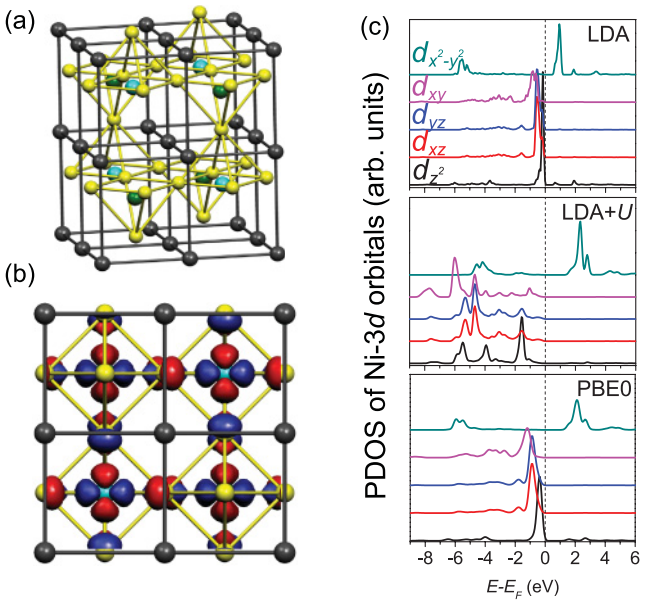

FIG. 6. (Color online) (a) Atomic structure of rocksalt B-site ordered Pb_2NiTiO_5. A 2 × 2 × 2 supercell containing 36 atoms is shown for clarity. (b) Isosurface of LUMO band (LDA results) at Γ. It is mainly composed of $d_{x^2-y^2}$ orbitals, displaying antibonding character between Ni-3$d_{x^2-y^2}$ and O-2p_z. (c) PDOS for Ni-3d orbital, obtained using LDA, LDA + U, and PBE0 functional calculations, respectively.

After exploring the electronic properties of the layered structure, we extend our investigation to rocksalt ordered Ni-PTO [Fig. 6(a)]. In the layered structure, there is a strong *bonding* character between Ni-$d_{x^2-y^2}$ and O-p_z (at Γ). However, in rocksalt Ni-PTO, there is an *antibonding* relation between Ni-$d_{x^2-y^2}$ and O-p_z, while bonding with O-p_z occurs almost exclusively between Ti and O [Fig. 6(b)]. This hybridization pattern indicates that the electron density is shared mainly between Ti-3d and O-2p, and that the Ni-$d_{x^2-y^2}$ orbital is almost empty. This leads to the prediction of a semiconducting ground state for rocksalt ordered Ni-PTO, even at the LDA level [Fig. 6(c)]. A consistent picture emerges, as LDA + U, PBE0, and sc-GW all predict rocksalt Pb_2NiTiO_5 to be a semiconductor.

Besides the Ni-$d_{x^2-y^2}$ orbital, other Ni-d bands also differ between the rocksalt and layered structures of Ni-PTO. In layered Ni-PTO, a strong hybridization between Ni and O yields energy bands with a large bandwidth. However, in rocksalt Ni-PTO, interrupting the NiO_2 layer with Ti-O cages makes it more favorable for the filled O-2p orbitals to mix with the empty 3d orbitals of Ti^{4+}.[47] Therefore, the Ni-3d orbital is weakly hybridized with O-2p, reducing its bandwidth in rocksalt Ni-PTO [Fig. 6(c)].

D. *B*-site cation ordering effects

The results of our electronic band-structure analysis indicate that different B-site cation orderings for Pb_2NiTiO_5 systems can give rise to different degrees of Ni-O bond covalency. To support this, we calculate the Born effective charges (BECs) for B-site cations of Ni-PTO.

Since the LDA incorrectly predicts a metallic ground state for layered Ni-PTO, the BECs and polarization $\vec{P}$ of Ni-PTO should be calculated at the post-DFT level. The BEC tensor, $Z^*_{\kappa,\alpha\beta}$, is defined as the change in the macroscopic polarization along direction α in response to a rigid displacement of a sublattice of atoms κ in direction β, times the unit-cell volume Ω_0:[48]

$$Z^*_{\kappa,\alpha\beta} = \Omega_0 \frac{\partial P_\alpha}{\partial \tau_{\kappa,\beta}}\bigg|_{\vec{E}=0} \cong \Omega_0 \frac{\Delta P_\alpha}{\Delta \tau_{\kappa,\beta}}\bigg|_{\vec{E}=0}. \quad (3)$$

Following this definition, Z^* can be estimated by the finite-difference method: each atom κ is displaced slightly from its equilibrium position by $\Delta\tau_\beta$, and the resulting change in polarization ΔP_α can be calculated using the Berry-phase method.[21,22] The displacement should be small enough to ensure the validity of the linear treatment of Eq. (3). For each structure, U is determined by a linear-response calculation, so that LDA + U calculations can generate an insulating ground state for all Ni-PTO structures. In this way, we calculate both Z^* and $\vec{P}$ at the LDA + U level.

Table III gives the calculated nonzero BECs for Ni ions in Ni-PTO systems. As the Ni^{2+} ion strongly favors a fourfold-coordinate environment, its planar BEC tensor elements (Z^*_{xx} and Z^*_{yy}) are larger than its nominal charge, indicative of covalency for the planar Ni-O bonds. Since the apical O moves away from Ni to create a square planar environment, the bonding between Ni and the apical O is weak. In the finite-difference simulation of Z^*, when the Ni ion moves

TABLE III. The Born effective charges Z^* of Ni cations in Ni-PTO solid solutions. Z^* is calculated using LDA + U finite-difference methods.

Composition	Z^*_{xx}	Z^*_{yy}	Z^*_{zz}
$1 \times 1 \times 2$ Pb_2NiTiO_5	2.29	2.29	0.44
$1 \times 1 \times 3$ $Pb_3NiTi_2O_8$	2.33	2.33	0.37
rocksalt Pb_2NiTiO_5	2.14	2.14	0.86
$\sqrt{2} \times \sqrt{2} \times 2$ $Pb_4NiTi_3O_{11}$	2.17	2.17	0.72
$2 \times 2 \times 2$ $Pb_8NiTi_7O_{23}$	2.15	2.15	0.78

closer to the apical O, the electron density will transfer from Ni to O. Because of this negative charge-density flow, the Ni ion will have a Z^*_{zz} smaller than its nominal charge. Moreover, the following trend is identified: as B-site cations change from layered to rocksalt ordering, there is decrease of the in-plane BEC tensor elements (Z^*_{xx} and Z^*_{yy}) of Ni and an increase of Z^*_{zz} along the Ni-O vacancy direction. This trend is in good agreement with the bond covalency results we obtained above, which indicate that layered Ni-PTO has a more covalent Ni-O bond and larger Z^*_{xx} and Z^*_{yy} values for Ni, while a less covalent Ni-O bond in rocksalt structure leads to the smaller in-plane Ni BECs.

In perovskite ABO_3 compounds, a more ionic B-O bond usually yields a larger E_g, while a more covalent B-O bond is associated with a smaller E_g. This trend has been verified for many perovskite systems, such as $Pb(Zr_xTi_{1-x})O_3$ (Ref. 49) and sulfide perovskite $BaZrS_3$.[50] In light of this trend, we now examine the Ni-PTO solid solution systems.

E_g of several Ni-PTO solid solutions are summarized in Table IV. Relative to PTO, E_g of Ni-PTO solid solutions are considerably reduced. For the rocksalt structure, LDA + U, PBE0, and sc-GW calculations increase E_g (relative to the LDA) by different amounts, and the trend in calculated E_g is LDA < LDA + U < PBE0 < sc-GW. Unlike the parameter-free sc-GW, E_g results obtained from LDA + U and PBE0 depend fairly strongly on the computational parameters (exact-exchange mixing fraction α for PBE0 and Hubbard U term for LDA + U). In the present work, LDA + U and PBE0 E_g are in good agreement with sc-GW results, verifying our parametrization for these calculations. It is worth noting that even though LDA + U yields E_g similar to PBE0 and sc-GW, LDA + U gives a more localized and perhaps less realistic DOS distribution [Fig. 5(a) and Ref. 51]. Therefore, we only use it to obtain the relative E_g trend, but we do not rely on LDA + U for the precise electronic structure. Our calculated E_g exhibits obvious B-site ordering effects: layered Ni-PTO always has a smaller E_g than rocksalt ordered Ni-PTO, and the variation in Ni doping percentage has little impact on the E_g value.

By comparing the BEC tensor and E_g results of Ni-PTO solid solutions, we can establish the relationship between B-site cation ordering and band gap. The electronic properties of Ni-PTO depend primarily on the Ni-O bonding. In layered Ni-PTO, there is a complete Ni-O-Ni network, and strong hybridization between Ni-d and O-p increases Ni-O bond covalency, yielding a smaller E_g. However, if the Ni-O-Ni network is interrupted by Ti-O bonds, the hybridization between the filled O-2p orbitals and the empty 3d orbitals of Ti^{4+} will be more favorable.[47] As a result, there is a more ionic bond between Ni-d and O-p, and the system has a larger E_g.

Guided by the E_g trend obtained above, we estimate that the lower E_g limit of Ni-PTO solid solutions should come from the layered structure, which could potentially be synthesized via layer-by-layer deposition techniques; the upper E_g limit corresponds to the more ionic rocksalt ordering structure, which can perhaps be obtained with a thermal annealing process. According to our prediction, layered Ni-PTO should have a direct optical band gap comparable to bulk Si, and E_g of rocksalt ordered Ni-PTO is close to that of $BiFeO_3$.[8] In this way, Ni-PTO solid solutions should have direct band gaps in the visible light energy range, displaying semiconducting electronic properties.

IV. CONCLUSION

In conclusion, we present theoretical studies on the electronic properties of $Pb(Ni_xTi_{1-x})O_{3-x}$ solid solutions. We identify the relation between B-site cation ordering and E_g of Ni-PTO systems. We expect that this relation can be used as a guiding principle to understand E_g behaviors for many perovskite solid solutions. Based on our theoretical calculations, we predict that the Ni-PTO solid solution can offer both a large polarization and a direct band gap in the visible light energy range. This combination of properties indicates that high photovoltaic efficiency can be realized in solar devices based on $Pb(Ni_xTi_{1-x})O_{3-x}$ oxides.

Furthermore, we demonstrate that the standard DFT-LDA provides a qualitatively incorrect electronic structure for

TABLE IV. Reported here are the c/a ratio, polarization P (in C/m^2), as well as indirect E_g (in eV) calculated using different methods for all the Ni-PTO solid solutions under investigation. Also shown are tetragonal $PbTiO_3$ results. For Ni-PTO solid solutions, direct band gaps at Γ are given in parentheses. Structural parameters are obtained by LDA calculations, and P is calculated using the LDA + U finite-difference method. We use the optimal α for PBE0 calculation.

Composition	c/a	P	E_g^{LDA}	E_g^{LDA+U}	E_g^{PBE0}	$E_g^{sc\text{-}GW}$
$PbTiO_3$	1.05	0.81	1.46(3.05)	2.17(3.80)	3.50(4.31)	3.90(5.80)
$1 \times 1 \times 2$ Ni-PTO	1.14	0.85	0.00(0.00)	0.70(1.19)	0.87(1.02)	
$1 \times 1 \times 3$ Ni-PTO	1.14	0.84	0.00(0.00)	0.52(1.57)		
rocksalt Ni-PTO	1.21	0.96	0.69(1.12)	1.59(2.65)	1.71(2.64)	1.83(2.70)
$\sqrt{2} \times \sqrt{2} \times 2$ Ni-PTO	1.12	0.90	0.84(0.97)	1.53(2.24)		
$2 \times 2 \times 2$ Ni-PTO	1.08	0.83	0.70(0.94)	1.60(1.90)		

layered Ni-PTO, and potentially other systems being investigated as possible components in solar harvesting devices. A more accurate treatment of the Ni-3*d* states of Ni-PTO required post-DFT LDA calculations to obtain reasonable band gaps. Of the work presented here, the LDA + U method is the least computationally expensive of the post-DFT methods, although it sometimes yields unreasonable crystal-field splits and unphysical PDOS features. Though it is the most computationally demanding, sc-GW yields band-gap results that are closest to experiment. The band-gap results of PBE0 are close to that of sc-GW and reproduce salient spectral features of the PDOS, while the computational cost is far less than that of GW. For the purposes of calculating accurate band gaps, we suggest that the PBE0 method is a reasonable compromise of accuracy and cost.

ACKNOWLEDGMENTS

G.Y.G. and J.W.B. were supported by the Department of Energy Office of Basic Energy Sciences under Grant No. DE-FG02-07ER46431, and H.T. and A.M.R. were supported by the Office of Naval Research under Grant No. N00014-09-1-0157. The authors would like to acknowledge K. M. Rabe and D. R. Hamann for helpful scientific discussions during preparation of the paper. Computational support was provided by a DURIP grant and a Challenge Grant from the HPCMO.

[1] V. K. Yarmarkin, B. M. Gol'tsman, M. M. Kazanin, and V. V. Lemanov, Phys. Solid State **42**, 511 (2000).
[2] K. K. Uprety, L. E. Ocola, and O. Auciello, J. Appl. Phys. **102**, 084107 (2007).
[3] Y. Inoue, K. Sato, K. Sato, and H. Miyama, J. Phys. Chem. **90**, 2809 (1986).
[4] A. M. Glass, D. V. D. Linde, and T. J. Negran, Appl. Phys. Lett. **25**, 233 (1974).
[5] P. S. Brody, Solid State Commun. **12**, 673 (1973).
[6] J. Wang *et al.*, Science **299**, 1719 (2003).
[7] J. B. Neaton, C. Ederer, U. V. Waghmare, N. A. Spaldin, and K. M. Rabe, Phys. Rev. B **71**, 014113 (2005).
[8] S. R. Basu, L. W. Martin, Y. H. Chu, M. Gajek, R. Ramesh, R. C. Rai, X. Xu, and J. L. Musfeldt, Appl. Phys. Lett. **92**, 091905 (2008).
[9] A. J. Hauser, J. Zhang, L. Mier, R. A. Ricciardo, P. M. Woodward, T. L. Gustafson, L. J. Brillson, and F. Y. Yang, Appl. Phys. Lett. **92**, 222901 (2008).
[10] S. Y. Yang *et al.*, Appl. Phys. Lett. **95**, 062909 (2009).
[11] T. Choi, S. Lee, Y. Choi, V. Kiryukhin, and S.-W. Cheong, Science **324**, 63 (2009).
[12] J. W. Bennett, I. Grinberg, and A. M. Rappe, J. Am. Chem. Soc. **130**, 17409 (2008).
[13] J. W. Bennett, I. Grinberg, P. K. Davies, and A. M. Rappe, Phys. Rev. B **82**, 184106 (2010).
[14] V. I. Anisimov, J. Zaanen, and O. K. Andersen, Phys. Rev. B **44**, 943 (1991).
[15] P. Giannozzi *et al.*, J. Phys. Condens. Matter **21**, 395502 (2009).
[16] X. Gonze *et al.*, Comp. Mater. Sci. **25**, 478 (2002).
[17] H. J. Monkhorst and J. D. Pack, Phys. Rev. B **13**, 5188 (1976).
[18] A. M. Rappe, K. M. Rabe, E. Kaxiras, and J. D. Joannopoulos, Phys. Rev. B **41**, 1227 (1990).
[19] N. J. Ramer and A. M. Rappe, Phys. Rev. B **59**, 12471 (1999).
[20] [http://opium.sourceforge.net].
[21] R. Resta, Rev. Mod. Phys. **66**, 899 (1994).
[22] R. D. King-Smith and D. Vanderbilt, Phys. Rev. B **47**, 1651 (1993).
[23] M. S. Hybertsen and S. G. Louie, Phys. Rev. Lett. **55**, 1418 (1985).
[24] M. S. Hybertsen and S. G. Louie, Phys. Rev. B **34**, 5390 (1986).
[25] M. Cococcioni and S. de Gironcoli, Phys. Rev. B **71**, 035105 (2005).
[26] J. P. Perdew, M. Ernzerhof, and K. Burke, J. Chem. Phys. **105**, 9982 (1996).
[27] J. P. Perdew, K. Burke, and M. Ernzerhof, Phys. Rev. Lett. **77**, 3865 (1996).
[28] J. Paier, M. Marsman, K. Hummer, G. Kresse, I. C. Gerber, and J. G. Angyan, J. Chem. Phys. **124**, 154709 (2006).
[29] A. Alkauskas, P. Broqvist, F. Devynck, and A. Pasquarello, Phys. Rev. Lett. **101**, 106802 (2008).
[30] G. Shirane, R. Pepinsky, and B. C. Frazer, Acta Crystallogr. **9**, 131 (1956).
[31] A. K. Cheetham and D. A. O. Hope, Phys. Rev. B **27**, 6964 (1983).
[32] G. A. Sawatzky and J. W. Allen, Phys. Rev. Lett. **53**, 2339 (1984).
[33] L. Hedin, Phys. Rev. **139**, A796 (1965).
[34] S. Lebegue, B. Arnaud, M. Alouani, and P. E. Bloechl, Phys. Rev. B **67**, 155208 (2003).
[35] F. Bruneval, N. Vast, and L. Reining, Phys. Rev. B **74**, 045102 (2006).
[36] V. I. Anisimov, *Strong Coulomb Correlations in Electronic Structure Calculations* (Gordon and Breach, Amsterdam, The Netherlands, 2000).
[37] T. M. Schuler, D. L. Ederer, S. Itza-Ortiz, G. T. Woods, T. A. Callcott, and J. C. Woicik, Phys. Rev. B **71**, 115113 (2005).
[38] J. Kunes, V. I. Anisimov, S. L. Skornyakov, A. V. Lukoyanov, and D. Vollhardt, Phys. Rev. Lett. **99**, 156404 (2007).
[39] F. A. Kröger and H. J. Vink, Solid State Phys. **3**, 307 (1956).
[40] V. I. Anisimov, D. Bukhvalov, and T. M. Rice, Phys. Rev. B **59**, 7901 (1999).
[41] D. I. Bilc, R. Orlando, R. Shaltaf, G.-M. Rignanese, J. Íñiguez, and P. Ghosez, Phys. Rev. B **77**, 165107 (2008).
[42] W. G. Schmidt, M. Albrecht, S. Wippermann, S. Blankenburg, E. Rauls, F. Fuchs, C. Rödl, J. Furthmüller, and A. Hermann, Phys. Rev. B **77**, 035106 (2008).
[43] S. Sanna, C. Thierfelder, S. Wippermann, T. P. Sinha, and W. G. Schmidt, Phys. Rev. B **83**, 054112 (2011).
[44] Y. Nohara, S. Yamamoto, and T. Fujiwara, Phys. Rev. B **79**, 195110 (2009).
[45] T. Kotani and H. Kino, J. Phys. Condens. Matter **21**, 266002 (2009).
[46] M. Oshikiri, M. Boero, J. Ye, F. Aryasetiawan, and G. Kido, Thin Solid Films **445**, 168 (2003).
[47] R. A. Wheeler, M. H. Whangbo, T. Hughbanks, R. Hoffmann, J. K. Burdett, and T. A. Albrightl, J. Am. Chem. Soc. **108**, 2222 (1986).
[48] P. Ghosez, J.-P. Michenaud, and X. Gonze, Phys. Rev. B **58**, 6224 (1998).
[49] H. Lee *et al.*, J. Appl. Phys. **98**, 094108 (2005).
[50] J. W. Bennett, I. Grinberg, and A. M. Rappe, Phys. Rev. B **79**, 235115 (2009).
[51] See supplemental material at [http://link.aps.org/supplemental/10.1103/PhysRevB.83.205115] for detailed analysis of orbital energy levels of layered Ni-PTO, predicted by LDA, LDA + U, and PBE0 calculations.